THE JOURNAL OF BIOLOGICAL CHEMISTRY VOL. 291, NO. 41, pp. 21375–21387, October 7, 2016

Subversion of Schwann Cell Glucose Metabolism by *Mycobacterium leprae*[*]

Received for publication, March 2, 2016, and in revised form, August 11, 2016 Published, JBC Papers in Press, August 23, 2016, DOI 10.1074/jbc.M116.725283

Rychelle Clayde Affonso Medeiros[‡], Karina do Carmo de Vasconcelos Girardi[‡], Fernanda Karlla Luz Cardoso[‡], Bruno de Siqueira Mietto[§], Thiago Gomes de Toledo Pinto[§], Lilian Sales Gomez[¶], Luciana Silva Rodrigues[‖], Mariana Gandini[‡], Julio Jablonski Amaral[**], Sérgio Luiz Gomes Antunes[§], Suzana Corte-Real[‡‡], Patricia Sammarco Rosa[§§], Maria Cristina Vidal Pessolani[‡], José Augusto da Costa Nery[§], Euzenir Nunes Sarno[§], Leonardo Ribeiro Batista-Silva[§], Mauro Sola-Penna[¶], Marcus Fernandes Oliveira[¶¶], Milton Ozório Moraes[§], and Flavio Alves Lara[‡1]

From the Laboratório de [‡]Microbiologia Celular, [‡‡]Biologia Estrutural, and [§]Hanseníase, Oswaldo Cruz Institute, Fiocruz, Rio de Janeiro-RJ, the Laboratório de [¶]Enzimologia e controle do metabolismo and [‖]Imunopatologia, Medical Science Faculty, Rio de Janeiro State University, Rio de Janeiro-RJ, the [**]National Institute of Metrology, Quality and Technology INMETRO, Rio de Janeiro-RJ, the [§§]Department of Biology, Lauro de Souza Lima Institute, Bauru-SP, and the [¶¶]Laboratório de Bioquímica de Resposta ao Estresse, Federal University of Rio de Janeiro, Rio de Janeiro, Brazil

***Mycobacterium leprae*, the intracellular etiological agent of leprosy, infects Schwann promoting irreversible physical disabilities and deformities. These cells are responsible for myelination and maintenance of axonal energy metabolism through export of metabolites, such as lactate and pyruvate. In the present work, we observed that infected Schwann cells increase glucose uptake with a concomitant increase in glucose-6-phosphate dehydrogenase (G6PDH) activity, the key enzyme of the oxidative pentose pathway. We also observed a mitochondria shutdown in infected cells and mitochondrial swelling in pure neural leprosy nerves. The classic Warburg effect described in macrophages infected by *Mycobacterium avium* was not observed in our model, which presented a drastic reduction in lactate generation and release by infected Schwann cells. This effect was followed by a decrease in lactate dehydrogenase isoform M (LDH-M) activity and an increase in cellular protection against hydrogen peroxide insult in a pentose phosphate pathway and GSH-dependent manner. *M. leprae* infection success was also dependent of the glutathione antioxidant system and its main reducing power source, the pentose pathway, as demonstrated by a 50 and 70% drop in intracellular viability after treatment with the GSH synthesis inhibitor buthionine sulfoximine, and aminonicotinamide (6-ANAM), an inhibitor of G6PDH 6-ANAM, respectively. We concluded that *M. leprae* could modulate host cell glucose metabolism to increase the cellular reducing power generation, facilitating glutathione regeneration and consequently free-radical control. The impact of this regulation in leprosy neuropathy is discussed.**

According to the World Health Organization, the number of new individuals diagnosed with leprosy in 2014 remained stable at 213,899 worldwide (1). Although it is an ancient disease, the molecular and cellular mechanisms underlying leprosy are still poorly understood. Moreover, this disease encompasses a complex and broad clinical and immunopathological spectrum, characterized by severe peripheral nerve demyelination and extensive axonal loss, the most recognized hallmarks of the disease, resulting in impairment of neural function, disfigurement, and deformities. Leprosy is not considered a fatal disease, but it is still responsible for more than 14,000 cases of irreversible motor disability and deformity globally per year (1).

The constant increase in the numbers of dapsone-resistant *Mycobacterium leprae* isolates along decades led the World Health Organization to implement multidrug therapy in 1982, using a rifampicin, dapsone, and clofazimine combination to treat leprosy. Although implementation of multidrug therapy by World Health Organization reduced the prevalence of the disease worldwide, its eradication appears distant, mainly because the number of new cases reported annually in endemic areas remains stable (2). The development of an improved multidrug therapy using not only antibiotics but also drugs that act by modulating the host metabolism against infection, such as addition of statins to the current multidrug therapy could be a promising strategy to reduce disease burden (3).

Evolutionary analysis indicates that *M. leprae* underwent a large reduction in gene content along with its specialization to primarily infect human cells, specifically Schwann cells and macrophages. This genetic decay resulted in the loss of almost half of its genome, although spared genes related to energy metabolism, specifically those involved in glucose anabolism and catabolism and lipid anabolism (4). The loss of genes required for growth using lipids as the sole carbon source is believed to cause the *M. leprae* dependence on host glucose intermediates to survive (4). Recently we have demonstrated that *M. leprae* infection in Schwann cells activates Toll-like receptor-6, resulting in induction of the PI3K pathway and *de novo* lipid synthesis and uptake from the medium (5). It is believed that the subversion of host cell lipid metabolism and formation of droplets is a *M. leprae* strategy for infection and persistence (6) based on the fact that lipid bodies are related to the production of immunomodulators such as prostaglandin E_2 (7).

[*] The authors declare that they have no conflicts of interest with the contents of this article.

[1] To whom correspondence should be addressed: Pavilhão Hanseníase, Instituto Oswaldo Cruz, Fundação Oswaldo Cruz, Av. Brasil, 4365, sala 27. 21040-360 Rio de Janeiro, RJ, Brazil. Tel.: 5521-2562-1552; E-mail: flavioalveslara2000@gmail.com.

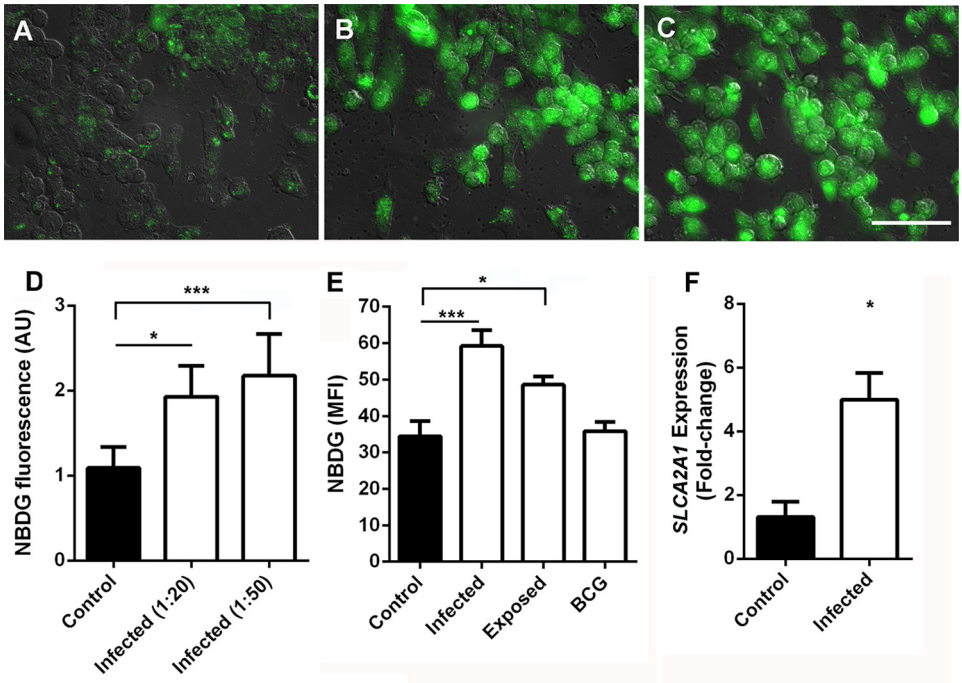

FIGURE 1. ***M. leprae* infection increases glucose uptake by Schwann cells.** Glucose uptake was determined by measuring 2-NBDG (a glucose analog) fluorescence intensity by fluorescence microscopy (*A–D*) and flow cytometry (*E*). Representative fields from control Schwann cell cultures (*A*). *M. leprae*-infected cells at an m.o.i. of 20:1 (*B*) and 50:1 (*C*) were acquired, and the rate between fluorescence mean and number of cells was determined (*D*). In *E*, fluorescence intensity medians were obtained by flow cytometry of infected, lethally irradiated *M. leprae*-stimulated Schwann cells or live BCG. Nonspecific binding of the glucose analog was observed as minimal at 4 °C and was deducted from the uptake at 37 °C. *F*, Glut-1 transporter (SLC2A1) expression induction by *M. leprae* in Schwann cells. The results are expressed as the mean ± S.E. from three normalized independent biological replicates. Statistical significance was calculated by ANOVA followed by the Bonferroni test where, ***, $p < 0.001$, and *, $p < 0.05$ are shown in comparison to the control. *Scale bar* = 50 μm.

The pentose phosphate pathway (PPP,[2] also called phosphogluconate pathway or hexose monophosphate shunt) is a metabolic signaling pathway parallel to glycolysis that generates NADPH and ribose 5-phosphate as the main products, representing the source of cellular reducing power responsible for lipid synthesis and glutathione antioxidant system maintenance as well as generation of DNA and RNA precursors. There are two distinct phases in the pathway: the oxidative, in which glucose-6-phosphate dehydrogenase (G6PDH) activity is the limiting enzyme required to generate NADPH, and the second phase, represented by the non-oxidative synthesis of carbon sugars (8). There are numerous mutations that can cause a G6PDH deficiency resulting in neonatal jaundice and hemolytic anemias induced by drugs, diabetes, and infections (9). Some of these variations are relatively frequent among human population due to the positive impact on a large number of pathogens, conferring natural resistance against *Chlamydia trachomatis* and *Plasmodium falciparum* infections (10, 11). On the other hand, the PPP is related to increased cellular tolerance to *Staphylococcus aureus* and *Helicobacter pylori* (12, 13).

There is growing evidence for the crucial role of Schwann cells as the main support for energy production in axons (14). During catabolic processes, Schwann cell glycogen is converted into lactate, which is transported to the axon by monocarboxylate transporters (MCTs), oxidized to pyruvate, and inserted in the axonal Krebs cycle for ATP production (15).

In the present work, we demonstrated that *M. leprae* infection was able to modulate Schwann cell glucose metabolism, generating a marked increase in glucose uptake and the PPP oxidative cycle key enzyme G6PDH. In addition, *M. leprae* infection also reduced mitochondrion membrane potential and lactate release by Schwann cells. These alterations resulted in free-radical control. We also observed that inhibition of host G6PDH or glutathione reductase activity reduced *M. leprae* viability to 70 and 60%, respectively, demonstrating the potential of this pathway in the control of leprosy and possibly other mycobacterial infections, such as extensively drug-resistant tuberculosis.

Results

M. leprae Infection Changes Glucose Uptake and Mitochondrial Metabolism in Schwann Cells—To observe possible modulation in glucose uptake by Schwann cells during *M. leprae* infection, we determined cellular uptake of the green fluorescent glucose analog (2-NBDG) by fluorescence microscopy (Fig. 1, *A–D*) in *M. leprae*-infected Schwann cells. The results showed a dose-response correlation between *M. leprae* multiplicity of infection (m.o.i.) and increase in 2-NBDG cellular uptake (Fig. 1*D*). We were able to more precisely analyze 2-NBDG uptake by deducting unspecific membrane binding

[2] The abbreviations used are: PPP, pentose phosphate pathway; G6PDH, glucose-6-phosphate dehydrogenase; TMRM, tetramethylrhodamine methyl ester; CCCP, carbonyl cyanide *p*-chlorophenylhydrazone; 2-NBDG, 2-[*N*-(7-nitrobenz-2-oxa-1,3-diazol-4-yl)amino]-2-deoxy-D-glucose; AMA, antimycin A; LL, lepromatous leprosy; BT, borderline tuberculoid; GSR, glutathione-disulfide reductase; DHE, dihydroethidium; 6-ANAM, aminonicotinamide; BCG, bacille Calmette-Guerin; ROS, reactive oxygen species; BSO, buthionine sulfoximine; m.o.i., multiplicity of infection; PI, propidium iodide; ANOVA, analysis of variance.

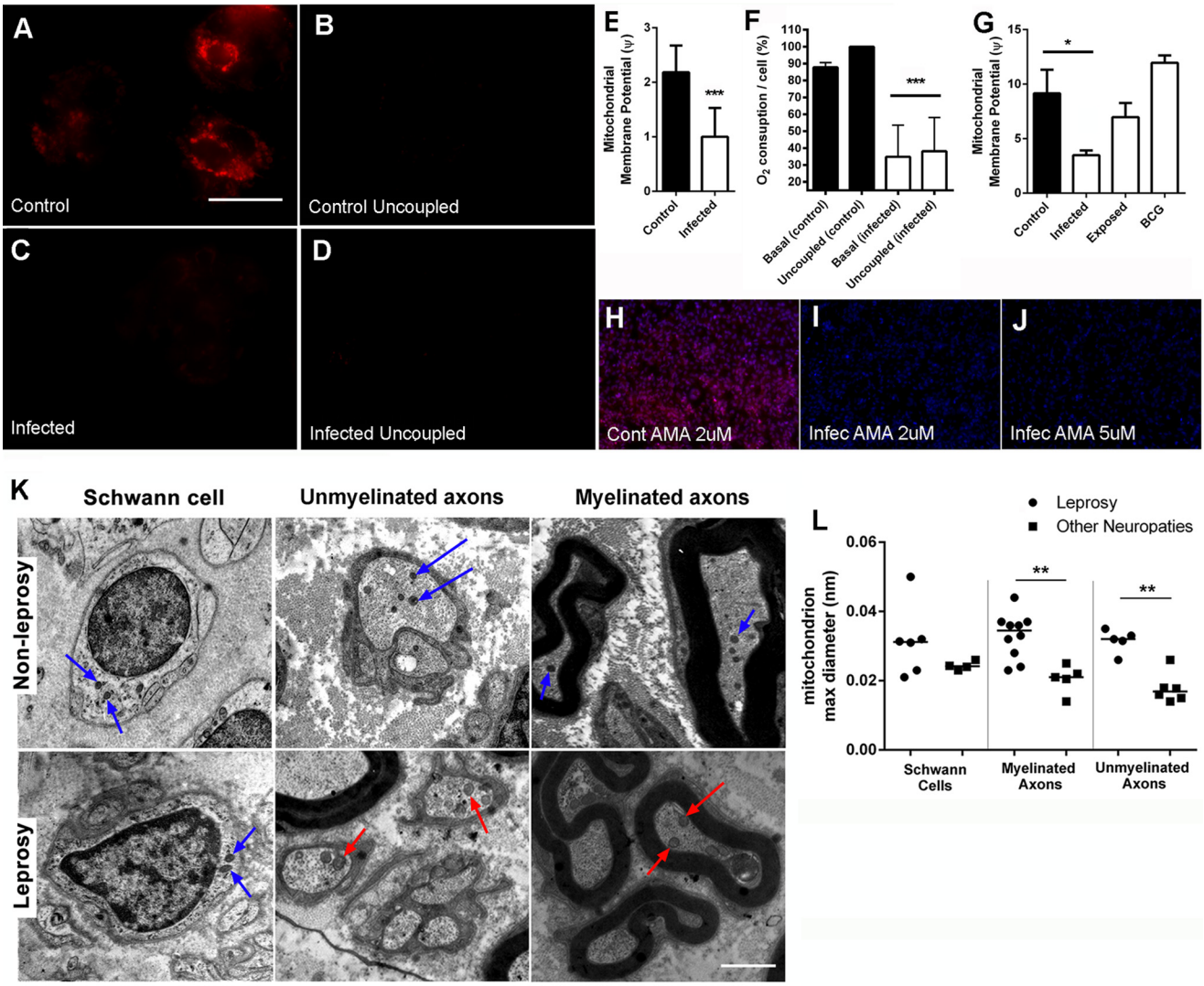

FIGURE 2. ***M. leprae* infection promotes mitochondrial membrane potential depolarization.** Mitochondrial membrane potential was determined by TMRM fluorescence intensity observed by fluorescence microscopy as coupled (*A–C*) and uncoupled by CCCP (*B–D*). Representative images from 120 fields were observed in three different replicates. *Scale bar* = 20 μm. The ratio between the coupled and uncoupled signal is a measure of the mitochondrial membrane potential (Ψ) shown in *E*. *F,* normalized oxygen consumption was determined with an oxygraph, where basal and uncoupled (CCCP) respiration rates were determined, assuming uncoupled control oxygen consumption as the maximal respiration rate in all experiments (100%). *G,* mitochondrial membrane potential was determined by measuring the fluorescence intensity ratio between cells exposed to TMRM and TMRM plus CCCP (uncoupled) by flow cytometry. The reduction in mitochondrial membrane potential induced by *M. leprae* infection is reflected as antimycin A desensitization by infected cells (*H–J*). Necrotic cell nuclei were stained by propidium iodide (*red*), and all nuclei were stained by DAPI (*blue*). As expected, control cells die after treatment with 2 μM antimycin A (*H*). In contrast, infected cells resist up to 5 μM antimycin A (*I* and *J*). Representative images were from 90 fields observed in three different replicates. *Scale bar* = 20 μm. Normal (*blue arrows*) and swelled mitochondria (*red arrows*) were observed by electron transmission microscopy (*K*). Mitochondria radiuses were determined in leprosy patients and patients suffering from other neuropathies, demonstrating that mitochondrial swelling could be observed in both myelinated and unmyelinated leprosy patient axons. Differences observed in Schwann cell mitochondria radius between leprosy and other non-leprosy neuropathy patients were not statistically significant. *Scale bar* = 1 μM. The mean mitochondria radiuses were determined by ImageJ (*L*). The results are expressed as the mean ± S.E. from three normalized independent biological replicates. Statistical significance was calculated by ANOVA followed by Bonferroni test where: ***, $p < 0.0001$, and *, $p < 0.01$.

(4 °C), from global uptake (37 °C), determining the fluorescence intensity medians by flow cytometry, identifying a role of *M. leprae* metabolites in this process, as cells stimulated by γ-irradiation-inactivated *M. leprae*, which preserves all antigens, was not able to generate the same stimulus with equal magnitude, nor was a non-pathogenic mycobacteria such as BCG (Fig. 1*E*). As indicated by real-time PCR analysis (Fig. 1*F*), the increase in glucose analog uptake during *M. leprae* infection is related to the increase in *SLC2A1* mRNA expression, which encodes the main glucose receptor in Schwann cells, the glucose transporter protein type 1 (Glut-1).

Many years ago, the German scientist Otto Warburg revealed that tumors have a reduction in aerobic metabolism and a parallel increase in glycolysis. This phenomenon has since been recognized as the Warburg effect, characterized as a metabolic shift that tumor cells display toward increased glycolysis along with a reduction in aerobic metabolism (16). We used the mitochondria potential membrane-sensible probe tetramethylrhodamine methyl ester (TMRM) to assess the mitochondrial depolarization resulting from *M. leprae* infection to measure mitochondrial activity (Fig. 2, *A* and *C*). To demonstrate that the TMRM signal is specific to mitochondria in our model, we

successfully eliminated TMRM fluorescence by uncoupling Schwann cell mitochondria using the ionophore CCCP (Fig. 2, *B* and *D*). Using the TMRM signal ratio between both stimuli (TMRM/TMRM + CCCP), we estimated the mitochondrial membrane potential (Ψ) of these cells (Fig. 2*E*), which showed that *M. leprae*-infected Schwann cells had a substantial Ψ reduction. This observation was confirmed using a Clark electrode to determine oxygen consumption during *M. leprae* infection. We observed that infected Schwann cells showed ~65% less oxygen consumption than the control cells and that this respiration drop was insensible to uncoupling by CCCP, indicating a deficiency in the respiratory chain complex proteins or substrates (Fig. 2*F*). A flow cytometry analysis corroborated these observations, indicating again that only live *M. leprae* is able to generate this Warburg-like effect in Schwann cells (Fig. 2*G*). In fact, respiration appeared to be almost abandoned by infected Schwann cells. We observed a high incidence of death in uninfected cells when exposed to 2 μM of the complex III inhibitor antimycin A (AMA), in contrast with *M. leprae*-infected cells, which showed high levels of resistance to 5 μM AMA (Fig. 2, *H–J*).

As shown in Fig. 2*K*, mitochondria in non-myelinated and myelinated axons in peripheral nerves of patients suffering from other non-leprosy neuropathies are relatively normal compared with leprosy patients. Morphometric analysis showed that the length of the mitochondrial major axis of myelinated and unmyelinated axons is statistically higher in the leprosy group, indicating mitochondrial swelling among these patients. In contrast, this difference was not observed in leprosy patients Schwann cells mitochondria (Fig. 2*L*).

M. leprae Infection Does Not Promote a Classical Warburg Effect—The classical Warburg effect, observed during *Mycobacterium avium* infection, for example (17), is followed by an increase in lactate generation and subsequent release to the medium (16). We assessed lactate release by Schwann cells infected by *M. leprae*, BCG, or stimulated by γ-inactivated *M. leprae* (Fig. 3*A*). Surprisingly, lactate levels did not increase in infected cells. On the contrary, we observed an ~50% decrease in lactate secretion in the supernatants by infected Schwann cells when compared with uninfected or unstimulated controls (Fig. 3*A*). Curiously, irradiated *M. leprae* or BCG-infected cells showed no alterations in lactate secretion. This effect was also detected in serum from multibacillary leprosy patients (LL), which presents a substantial amount of bacilli infecting the nerves and skin. A reduced level of lactate was noticed among these patients compared with either healthy volunteers or paucibacillary leprosy patients (BT), with reduced or even undetectable bacilli.

To understand the mechanism involved in *M. leprae* modulation of lactate levels, we determined the activity of both isoforms of lactate dehydrogenase, the LDH-H, able to convert lactate to pyruvate, and the LDH-M isoform, able to convert pyruvate to lactate (Fig. 3, *C* and *D*). Although there was no difference observed in LDH-H activity, LDH-M activity is reduced in infected cells, and this could be an explanation for the reduction in lactate generation and release observed in these cells. The most feasible method to assess this phenomenon *in vivo* is to determine *LDH-B* and *LDH-A* gene expression levels in leprosy patients' skin lesion biopsies. These genes encode the LDH-H and LDH-M enzyme isoforms, respectively.

As shown in Fig. 3, *E* and *F*, LL patients present high levels of *LDH-B* and low levels of *LDH-A* when compared with BT patients. To corroborate this data, *LDH-A* gene expression from neural leprosy patients and patients suffering from other non-leprosy neuropathies nerve biopsies was determined (Fig. 3*G*). As expected, *LDH-A* expression was reduced in leprosy patient nerves. To confirm that the lactate levels drop in infected Schwann cells is related to a reduction in lactate production, and not lactate membrane transport inhibition, we determined the monocarboxylate transporters MCP 1, 2, and 4 expression, through determination of *SLC16A1, -3*, and *-7* mRNA abundance by real-time PCR (Fig. 3*H*). We observed that infected Schwann cells increased the expression of all three lactate transporters. Nerve fragments from leprosy patients showing high expression of *SLC16A7* compared with nerves biopsies from non-leprosy neuropathies patients (Fig. 3*I*).

M. leprae Infection Increases Glutathione Reductase Activity through Induction of the PPP—After the observation that *M. leprae*-infected Schwann cells present a glucose uptake increase followed by reduction in mitochondrial respiratory chain activity and a drop in lactate generation, we speculated that glucose would be diverted to the PPP in infected cells. To test this hypothesis, we determined G6PDH, the step-limiting enzyme of the PPP oxidative phase, expression (Fig. 4*A*) and activity (Fig. 4*B*) *in vitro* and *in vivo* (Fig. 4, *C* and *D*). *M. leprae* infection generated a 10-fold increase in *G6PDH* expression, resulting in doubled activity *in vitro*, indicating that glucose-6-P was more easily converted to ribulose 5-phosphate, a nucleic acid and amino acid precursor, than pyruvate and consequently lactate, generating NADPH during the process. The same seems to be true *in vivo*, where G6PDH expression was also increased in LL skin lesions compared with BT skin biopsies (Fig. 4*C*). G6PDH expression is also increased in peripheral nerves from leprosy patients when compared with other non-leprosy neuropathies nerve biopsies (Fig. 4*D*), corroborating the up-regulation of this pathway in the disease.

Phosphofructokinase 1 catalyzes the first committed step of glycolysis, and for this reason, its activity was determined *in vitro* (Fig. 4*E*). Phosphofructokinase 1 activity was not modulated during infection, indicating that glycolysis was not induced by *M. leprae*, similar to ATP abundance (Fig. 4*F*). On the other hand, malic enzyme, another important source of Schwann cell NADPH, showed up-regulated expression and activity *in vitro* (Fig. 4, *G* and *H*). Malic enzyme expression was also increased in peripheral nerves from leprosy patients compared with nerve biopsies from patients presenting non-leprosy-related neuropathies (Fig. 4*I*).

Lipid synthesis, one of the main destinations of cellular NADPH, is known to be increased during Schwann cell infection by *M. leprae* (6). ATP citrate lyase, which converts citrate to acetyl-CoA, is involved in the first step of the lipid synthesis pathway and is also increased in infected Schwann cells (Fig. 4*J*). The enzyme glutathione-disulfide reductase (GSR), which is involved in regeneration of oxidized glutathione to its reduced form, a crucial low molecular weight redox buffer in mammal cells, also utilizes NADPH and would potentially confer an

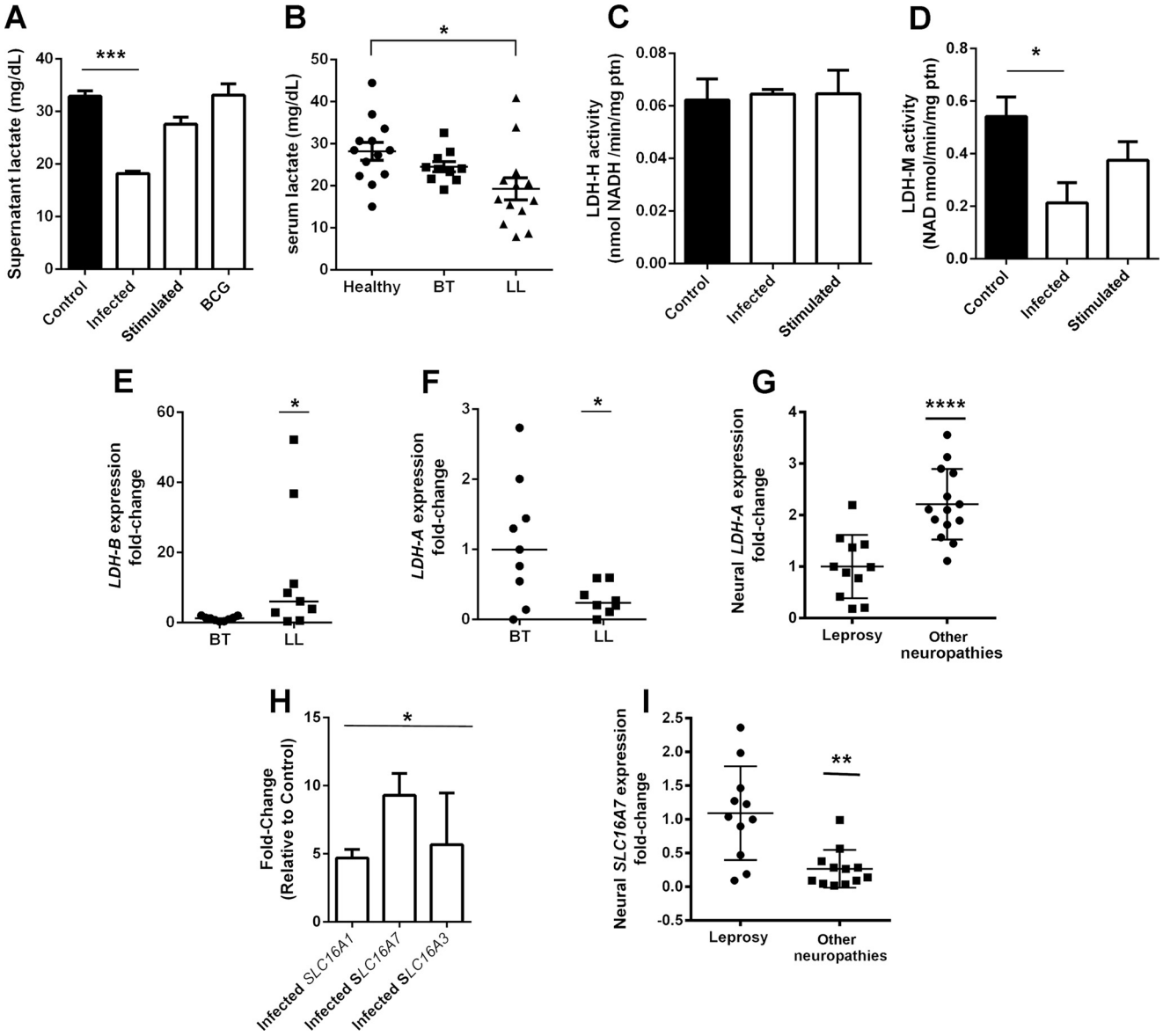

FIGURE 3. **Schwann cell lactate release is affected during *M. leprae* infection.** Lactate release in infected Schwann cell supernatant is reduced by half in comparison to control cells (*A*). Cells stimulated to BCG or *M. leprae* inactivated by radiation showed no reduction in lactate. Leprosy patients from the lepromatous pole of the disease (LL) also demonstrated a 30% reduction in serum lactate levels (*B*). Although Schwann cell lactate dehydrogenase isoform H activity is not affected (*C*), isoform M activity is reduced during *M. leprae* infection (*D*). LDH-B and LDH-A mRNA expression were determined in skin lesions from leprosy tuberculoid (*BT*) and lepromatous (*LL*) patients (*E* and *F*). LDH-A gene expression was determined in peripheral nerves biopsies from pure neural leprosy patients and patients suffering from other neuropathies (*G*). As expected, the LDH-A gene is repressed in leprosy patients. The monocarboxylate transporters SLC16A1, 16A3, and 16A7 are up-regulated in infected Schwann cells (*H*), whereas SLC16A3 is increased in peripheral nerves from leprosy patients in comparison to nerve biopsies from other neuropathies (*I*). The results are expressed as the mean ± S.E. from three normalized independent biological replicates. Statistical significance was calculated by ANOVA followed by Bonferroni test where: ***, $p < 0.0001$; **, $p < 0.001$; and *, $p < 0.01$ in comparison to control.

advantage for intracellular *M. leprae* growth (18). *GSR* mRNA expression was up-regulated *in vitro* and *in vivo* in Schwann cells, multibacillary (LL) skin lesions, and nerve biopsies (Fig. 4, *K–M*), indicating that *M. leprae* infection induces the glutathione generation system.

M. leprae Intracellular Viability Is Dependent on Host Cell Free-radical Defenses Maintained by Glutathione-disulfide Reductase and the PPP—Due to the increase in GSR activity during *M. leprae* infection, the next step was to determine whether infected Schwann cells are more resistant to oxidative insults due to the up-regulated PPP, which stimulates the glutathione system. We therefore monitored ST88-14 oxidative stress through the dihydroethidium (DHE) signal using FACS (Fig. 5).

M. leprae and BCG infection *per se* do not generate oxidative stress in ST88-14 Schwann cells. However, treatment with 10 μM hydrogen peroxide induced a higher DHE signal in control and BCG than *M. leprae*-infected Schwann cells, indicating that *M. leprae* infection increase cellular antioxidant defenses. Host cell free-radical protection was totally abolished when GSR or G6PDH activity was inhibited by buthionine sulfoximine (BSO) or 6-ANAM, respectively (Fig. 6, *A* and *B*).

By blocking PPP using 6-ANAM or glutathione regeneration using BSO, we successfully reverted the metabolism modulation mediated by *M. leprae*, rescuing infected cells' lactate production and mitochondrial membrane potential to normal levels (Fig. 6, *A* and *B*). Host cell viability was not impacted by any

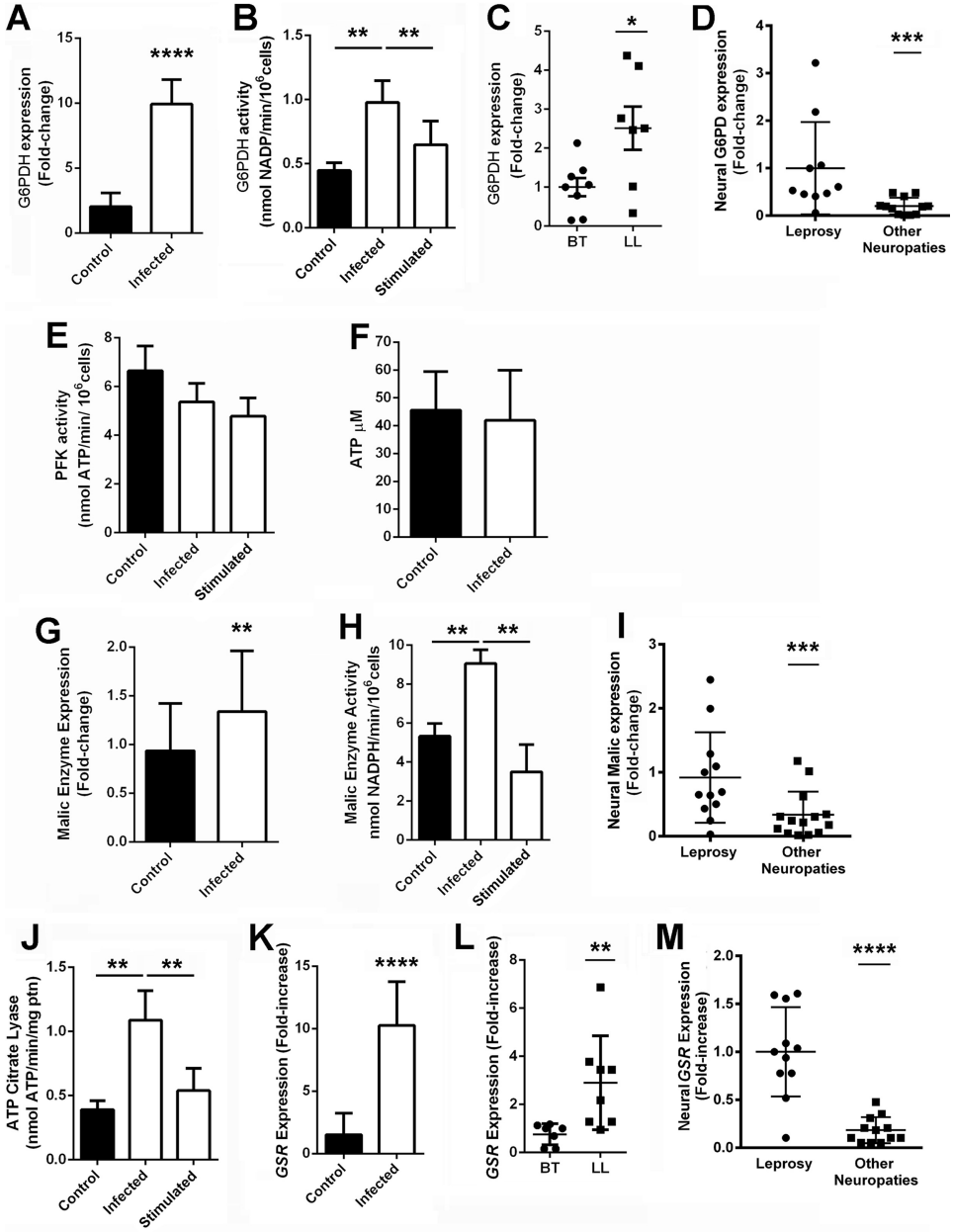

FIGURE 4. ***M. leprae* induces the Schwann cell pentose pathway oxidative phase.** G6PDH activity (*A*) and expression (*B*) is increased in infected Schwann cells. G6PDH expression is also increased in lepromatous leprosy skin lesions (*LL*), where *M. leprae* is abundant, compared with tuberculoid ones (*BT*) (*C*). G6PDH is also increased in peripheral nerves from leprosy patients when compared with nerve biopsies of other neuropathies (*D*). The PFK (*E*) and cellular ATP abundance (*F*) are not altered in infected Schwann cells. On the other hand, malic enzyme, another important source of Schwann cell reducing power, presented increased expression (*G*) and activity (*H*) during infection. Malic enzyme is also increased in peripheral nerves from leprosy patients when compared with nerve biopsies from patients diagnosed with other neuropathies not related with leprosy (*I*). ATP citrate lyase, the first enzyme of the lipid synthesis pathway, is also increased in infected Schwann cells (*J*). Glutathione reductase, the main destination of cell reducing power, is also increased during *M. leprae* infection in human Schwann cells (*K*), skin (*L*), and nerves (*M*). Cells incubated with γ-inactivated *M. leprae* are identified as stimulated. The results are expressed as the mean ± S.E. from three normalized independent biological replicates. Statistical significance was calculated by ANOVA followed by Bonferroni test where: ****, $p < 0.0001$; ***, $p < 0.001$; **, $p < 0.01$; and *, $p < 0.05$ in comparison to controls.

stimulus (data not shown), in contrast with *M. leprae* intracellular viability in Schwann cells. We observed that *M. leprae* viability is partially dependent on both host cell metabolic activities, observing a 50 and 70% drop in viability after 4 days of treatment with BSO and 6-ANAM, respectively (Fig. 6*C*). The impact of host cell G6PDH inhibition over *M. leprae* viability was confirmed by siRNA knockdown of the enzyme (Fig. 6*D*). Knockdown using siRNA 1 and 2 reduced *M. leprae* viability to 46 and 32%, respectively, in comparison with the scrambled siRNA control. These data demonstrate that host G6PDH is a new potential therapeutic target to control leprosy.

Discussion

In the present work, we described a profound metabolism modulation displayed by Schwann cells during *M. leprae* infection. We determined that this intracellular pathogen is able to subvert host cell metabolism by increasing cellular reducing power sources such as the PPP oxidative phase and malic

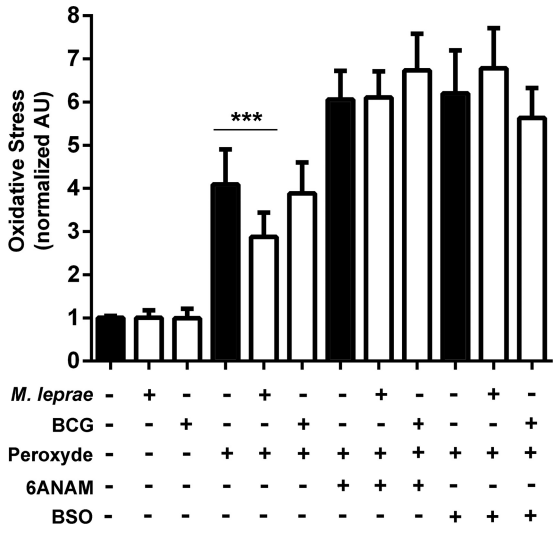

FIGURE 5. ***M. leprae* infection increases oxidative defenses of Schwann cells in a pentose pathway-dependent manner.** Schwann cells were infected by *M. leprae* or BCG (*white bars*) and challenged by hydrogen peroxide. Oxidative stress was measured by dihydroethidium fluorescence as determined by flow cytometry. Mycobacterial infection *per se* does not increase ROS in Schwann cells. On the contrary, *M. leprae* infection partially protects Schwann cells from hydrogen peroxide oxidative damage. The ROS protection was eliminated by G6PDH inhibitor 6-ANAM. The results are expressed as the mean ± S.E. from five normalized independent biological replicates. Statistical significance was calculated by ANOVA followed by Bonferroni test where: ***, $p < 0.0001$.

enzyme, down-regulating mitochondrial activity and drastically reducing lactate production by infected Schwann cells (Fig. 7).

The increased glucose utilization through aerobic glycolysis described by Warburg in neoplastic cells was subsequently found to occur *in vivo* in macrophages composing the granulomas of tuberculosis, as well as lymphocytes, an aerobic respiration to aerobic glycolysis switch (19). This observation is in accordance with the reduced oxygen tension expected to occur in nonvascularized caseating tuberculosis granulomas. The Warburg-like effect observed in *M. leprae*-infected Schwann cell was a surprise. Despite the drop in lactate released by infected cells, which is in contrast with the classical Warburg effect, *M. leprae*-infected Schwann cells displayed a reduction in mitochondrial membrane potential and respiration, presenting a mainly fermentative metabolism, as demonstrated by antimycin A resistance during infection.

It is likely that the mitochondria shutdown could be an *M. leprae* adaptation to reduce intracellular oxidative stress. In fact, a down-regulation of the mitochondrial respiratory chain genes after *M. leprae* infection has been reported (20). Despite the presence of various antioxidant defenses, the mitochondrion is recognized as the main intracellular source of reactive oxygen species (21). Various respiratory complexes leak electrons to oxygen, producing primarily superoxide anion and consequently raising hydrogen peroxide and peroxynitrite levels, which are both strong oxidants that indiscriminately react with nucleic acids, lipids, and proteins (22, 23). It is well known that uncoupling of mitochondria oxidative phosphorylation by uncoupling proteins strongly reduces mitochondrial ROS emission (24). By limiting electron pumping via citrate deviation to lipid synthesis, *M. leprae* drastically reduced host cell mitochondrial membrane potential and avoided ROS generation. This strategy could also be related to the early demyelination described in leprosy neuropathy because the Schwann cell Krebs cycle activity is important in differentiation and the myelination process (25).

Mitochondrial swelling is a hallmark of ultrastructural change occurring in damaged cells and is one of the most important indicators of the opening of the mitochondrial permeability transition pore, an event that, depending of the intensity of the insult, can lead to apoptosis (26–28). Although all mitochondrial modulations observed in the present work were performed in infected Schwann cells, we failed to observe mitochondrial swelling in ulnar and sural Schwann cells from leprosy patients. These data were expected because it is well known that *M. leprae* develops a series of mechanisms to avoid host cell apoptosis, such as insulin-like growth factor 1 up-regulation, for example (29). On the other hand, we observed swelling in myelinated and unmyelinated axonal mitochondria from leprosy patients' axonal fibers without any sign of inflammatory infiltrates, demyelination, or fibrosis, indicating that the mitochondria transition pore is opened and that this event may represent the first insult, which will result in neuronal death, the leprosy hallmark.

Probable ROS control is also involved in *M. leprae* adaptation to increase the activity of host G6PDH and malic enzyme, which together represent the main cellular sources of NADPH. The NADPH reducing power is consumed by glutathione reductase, which is also up-regulated during *M. leprae* infection, to maintain the glutathione antioxidant system. By inducing these two linked pathways, this obligatory intracellular pathogen is able to avoid host cell oxidative stress. This protection was eliminated by γ-glutamylcysteine synthetase or G6PDH inhibition by BSO or 6-ANAM, respectively, resulting in lactate regeneration and mitochondrial membrane potential restoration along with *M. leprae* loss of viability. Both pathways seem to be crucial to *M. leprae* infection, presenting potential new targets to control leprosy.

An important challenge to avoid leprosy demyelinating neurodegenerative neuropathy is to understand the cellular and molecular events that underlie the different phases of this process. *M. leprae* induces an intrinsic demyelination mechanism for nerve damage in leprosy, a process attributed to the immune response until then (30). Currently, leprosy neuropathy development is divided into two phases: the early events involving Schwann cell infection and intrinsic injury mechanisms and late events represented by the immune response mediating axonal damage and fibrosis (31).

We hypothesize that Schwann cells' lactate reduction could be an explanation for the axonal mitochondria swelling, representing a new mechanism of demyelination and neuronal death in leprosy neuropathy. The importance of glial cells' lactate to neuronal physiology has been largely characterized. Lee and collaborators (32), for example, observed axon damage and neuron loss *in vivo* and *in vitro* after disruption of glial cells' lactate transport to neurons in monocarboxylate transporter 1 knock-out animals. In addition to its well known metabolic role in sustaining synaptic function (33) and axonal activity (34),

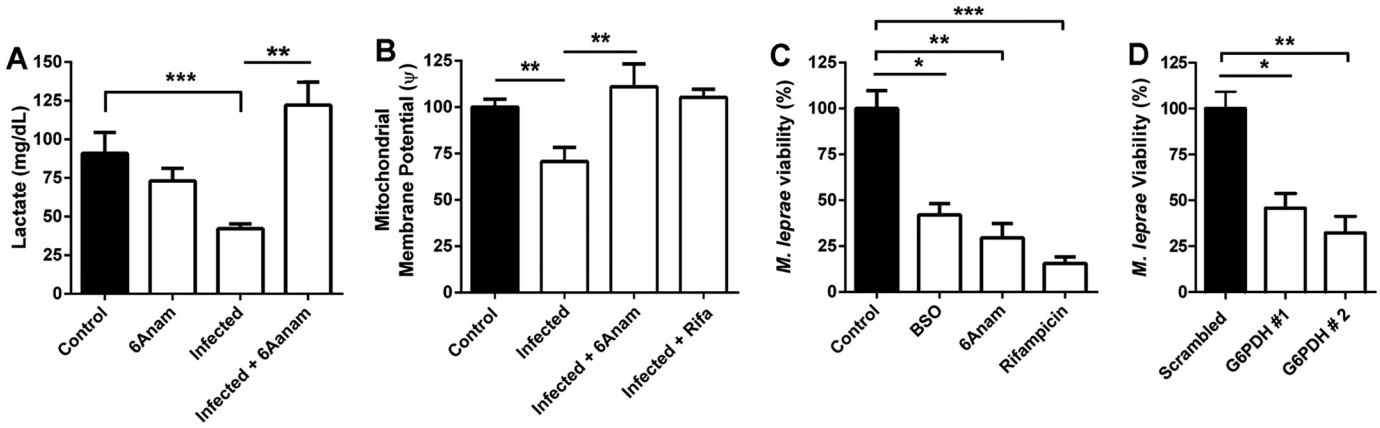

FIGURE 6. ***M. leprae* viability in Schwann cells is dependent on the pentose pathway.** *A,* the G6PDH inhibitor 6-ANAM recovers lactate production in *M. leprae*-infected Schwann cells. *B,* mitochondrial membrane potential, determined by the ratio of TMRM/TMRM + CCCP fluorescence signal by flow cytometry, was also recovered in infected Schwann cells by 6-ANAM and rifampicin. *C, M. leprae* intracellular viability was determined by real-time PCR 16S rRNA quantification. Schwann cells exposed to 6-ANAM or BSO were not able to maintain *M. leprae* infection *in vitro* for 5 days, similar to results in rifampicin. *D, M. leprae* viability was similarly impaired by G6PDH siRNA knockdown, after 2 days of infection. The results are expressed as the mean ± S.E. from three normalized independent biological replicates. Statistical significance was calculated by ANOVA followed by Bonferroni test where: ***, $p < 0.0001$; **, $p < 0.001$; and *, $p < 0.01$ in comparison to controls or between conditions when indicated.

lactate has been proposed to act as a neurotransmitter through specific receptors (35).

The difference between the classical Warburg effect, when an fermentative phenotype is followed by an increase in lactate generation, and the *M. leprae*-induced Warburg-like effect, represented by a reduction in respiration and lactate release by infected cells, could be explained by the decrease in lactate dehydrogenase M activity (Fig. 3, *D*, *F,* and *G*) and the increase in ATP citrate lyase activity. These results combined with the commitment of these carbons to pyruvate, citrate, and finally lipid synthesis, which is highly induced in infected Schwann cells under insulin-like growth factor-1/insulin signaling (6, 29), discarded the possibility of lactate consumption in gluconeogenesis.

More recently, it was demonstrated that *M. leprae* is able to generate neuropathy with consequent axonal death by down-regulating Schwann cell differentiation and myelination genes such as MBP, MPZ/P0, and Krox 20 (36). These observations could also be linked to the lactate synthesis drop observed in Schwann cells during *M. leprae* infection because it has already been demonstrated that myelination genes such as Krox20 and P0 are down-regulated in lactate-depleted Schwann cells (37). Hypophosphorylation in *M. leprae*-infected sciatic nerve neurofilament subunits results in a loss of axonal caliber and nerve conduction velocity (38). We believe that these observations could also be related to the reduction in lactate production in Schwann cells, which results in axonal lower Krebs cycle activity and a subsequent mitochondrial loss of function and swelling, leading to lower axonal energy production, global axonal metabolism reduction, neurofilament hypophosphorylation, and loss of neural conductivity (39).

To sum up, our data open the path to understanding the complex metabolic modulation of the host Schwann cells during *M. leprae* infection. The fermentative phenotype imposed on the host cell represents an increase in the oxidative defenses, likely associated with demyelination, due to the reduction in Schwann cell mitochondrial respiration and neuronal loss of conductivity due to lactate deprivation. We successfully reverted these effects in infected Schwann cells using 6-ANAM, with an impressive impact over *M. leprae* viability by silencing G6PDH. Curiously, both drugs are applied in cancer therapy (40). The potential of these new targets in leprosy neuropathy mitigation should be investigated. Our model pinpointed Schwann cell and *M. leprae* infection, but it could be hypothesized that other host cells could similarly respond to either *M. leprae* or other mycobacteria like *M. tuberculosis* in a way that XDR *M. tuberculosis*-infected patients could be benefited from this type of treatment.

Experimental Procedures

Cell Culture and Infection—The ST88-14 human Schwann cell line (kindly provided by Dr. Jonathan Fletcher, Harvard University, Boston, MA) was cultured in RPMI supplemented with 10% fetal bovine serum, 100 units/ml of penicillin, and 100 g/ml of streptomycin and maintained in a 5% CO_2 atmosphere. In all assays, unless otherwise stated, we carried out infection with *M. leprae* or *Mycobacterium bovis* BCG (*Moreau* strain) using a m.o.i. of 50 bacteria per cell (50:1) for 48 h at 33 °C in a 5% CO_2 atmosphere.

Treatment with Drugs—For reversing the effects of *M. leprae* infection, cells were exposed to different drugs interfering in fundamental metabolic pathways 24 h before infection: 5 μM 6-ANAM, an inhibitor of G6PDH; 400 μM BSO, an inhibitor of γ-glutamylcysteine synthetase; or antimycin A (2 μg/ml), an inhibitor of the electron transfer at complex III. All drugs, substrates, and fluorochrome used in the present work, unless otherwise stated, were purchased from Sigma.

Patients—A total of 84 not-treated patients: 20 paucibacillary (BT), 22 multibacillary (LL), 22 patients presenting pure neural leprosy, and 20 patients suffering from other non-diagnosed neuropathies, consisting of 44 males and 40 females from 25 to 88 years of age, were recruited from the Souza Araújo Service at the Oswaldo Cruz Foundation, Rio de Janeiro, Brazil, and classified according to the Ridley-Jopling scale and included in this study (Table 1). Ulnar and sural nerves biopsies were analyzed. The number of samples tested is not the same in different analysis because some of them did not present PCR amplification or did

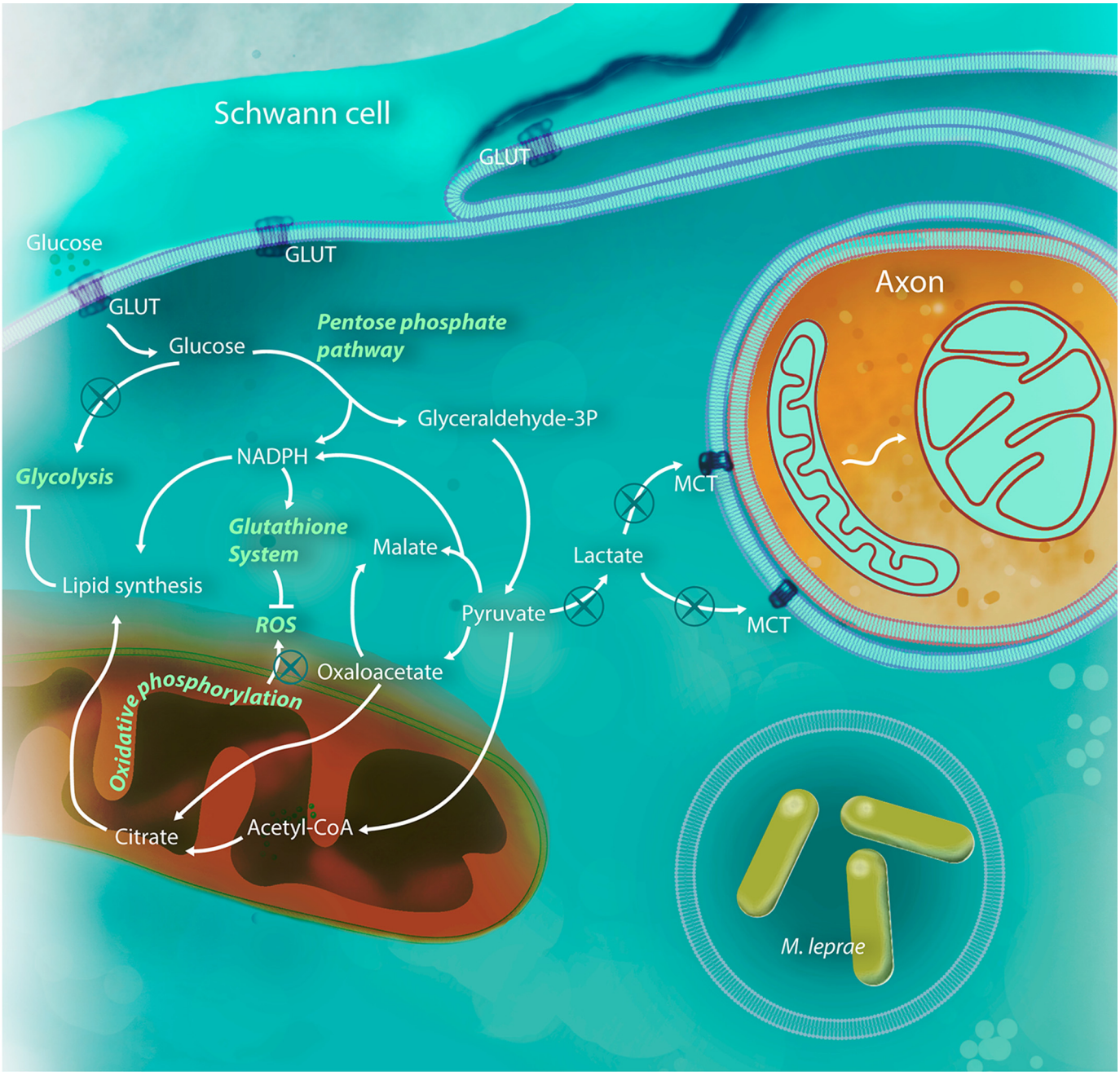

FIGURE 7. ***M. leprae* is able to modulate Schwann cell metabolism for its benefit.** After infection, Schwann cells increase glucose uptake, feeding the PPP with carbon, in detriment to glycolysis, probably due to phosphofructokinase inhibition by the increased levels of acyl-CoA in the cytoplasm. Pyruvate generated by PPP is converted to malate and acetyl-CoA instead of lactate, compromising axonal mitochondria physiology. Pyruvate is rapidly converted to citrate, increasing lipid synthesis and virtually stopping the Schwann cell tricarboxylic acid cycle and consequently respiratory chain and mitochondria energy potential. The NADPH generated by the oxidative phase of the PPP will maintain an up-regulated lipid synthesis and glutathione system. All three pathways are crucial to the success of *M. leprae* infection and could be used in new host-target therapy strategies.

not generate mitochondrial high resolution microscopic images in all three compartments: Schwann cells, myelinated and unmyelinated axons.

Mycobacteria Strains—Live *M. leprae* Thai-53 was prepared from athymic nu/nu mouse footpads immediately before use and was provided by Dr. Patricia Sammarco Rosa (Department of Biology, Lauro de Souza Lima Institute, Bauru-SP, Brazil). *M. leprae* preparation, viability determination, and purity were performed as described elsewhere (3). Part of the *M. leprae* suspension was killed by γ-irradiation in the Acelétron Facility (Rio de Janeiro, Brazil). *M. bovis* BCG Moreau was kindly provided by Carolina Cavareze (Fundação Ataulfo de Paiva, Rio de Janeiro, Brazil) and cultured in 7H9 Middlebrook medium supplemented with 0.02% glycerol, 10% ADC Middlebrook (BD Bioscience), and 0.05% Tween 80 (Difco Laboratories). Cultures were kept under constant agitation at 37 °C for 2 weeks. BCG was harvested in the mid-log phase, counted in a Petroff-Hausser chamber, and kept frozen at −70 °C until use.

Glucose Uptake and Lactate Measurement—Glucose uptake was monitored using the fluorescent glucose analog 2-NBDG

TABLE 1
Demographic and epidemiological data of individuals included in the study

Group	Samples	Assay	Individuals	Male	Female	Age (median)
			n			
Healthy	Serum	Lactate quantification	13	5	8	38.3
Pure neural leprosy	Nerve lesions	qRT-PCR	12	7	5	55.5
		TEM[a]	10	5	5	62
Other neuropathies	Nerve lesions	Quantitative RT-PCR	14	6	8	58
		TEM	6	3	3	42
BT	Serum	Lactate quantification	11	4	7	48
	Skin lesions	Quantitative RT-PCR	9	6	3	45
LL	Serum	Lactate quantification	13	9	4	36.5
	Skin lesions	Quantitative RT-PCR	9	4	5	46

[a] TEM, transmission electron microscopy.

(Sigma). After 48 h infection, round coverslip-adherent cells were exposed to the fluorophore at a concentration of 500 nM for 30 min in RPMI medium supplemented with 10% fetal bovine serum (FBS). Ten random fields per sample were acquired using a Zeiss AxioObserver inverted microscope with a Colibri illuminating system with Plan-Neofluar ×40 objective and a numerical aperture of 1.4 (Zeiss, Oberkochen, Germany). The green signal from NBDG was acquired by monochrome camera HMR Axiocan controlled by Axiovision software version 3.2 (Zeiss, Oberkochen, Germany). The illumination system used a 470-nm LED and Zeiss fluorescence filter 61. The cytometry analysis was performed as follow: after labeling and washing, cells were removed from the well with 0.125% trypsin and resuspended in cytometry buffer (10% FBS in PBS), placed on ice, and immediately subjected to the acquisition of 10,000 events with an AcuriC6 cytometer (BD Biosciences) in FL1 channel fluorescence. The results represent the rate between the fluorescence signal from 4 °C uptake (unspecific NBDG-2 membrane binding) and 37 °C uptake. Lactate quantification was performed from ST88-14 supernatants after 48 h infection by a m.o.i. of 50:1, using the Liquiform lactate kit (Labtest, Lagoa Santa, MG, Brazil) according to the manufacturer's instructions.

Electrical Potential Analysis of the Mitochondrial Membrane (ψ)—The electric mitochondrial membrane potential was determined by exposing ST88-14 cells to TMRM at 0.5 nM (Sigma). The results were shown by the ratio of the probe fluorescence signal to the same signal from a culture preincubated with the proton ionophore CCCP (Sigma). CCCP, titrated in our model using a curve from 5 to 70 μM, at 15 μM was recognized as the lower concentration able to deplete the TMRM signal, and for that reason, it was established as the concentration of choice. CCCP and antimycin A (2 mg/ml) were incubated 10 min prior to TMRM exposure. Cells were exposed to the probe for 10 min. For microscopy, we captured 10 random fields per sample using a Zeiss AxioObserver inverted microscope with a Colibri illuminating system and a Plan-Neofluar ×40 objective with a numerical aperture of 1.4 (Zeiss, Oberkochen, Germany). The red signal from TMRM was acquired by the monochrome camera HMR Axiocan controlled by Axiovision software version 3.2 (Zeiss, Oberkochen, Germany). The illumination system used a 530-nm LED and Zeiss fluorescence filter 50. Flow cytometry analysis were performed as follow: after labeling and washing, cells were then removed from the well with 0.125% trypsin and resuspended in cytometry buffer (10% FBS in PBS), placed on ice and immediately subjected to the acquisition of 10,000 events on FACSCalibur (BD Biosciences) FL2-fluorescence channel A.

Enzymatic Activity and ATP Quantification—Enzyme activities were assayed with 3×10^6 cells lysed in hypotonic buffer (25 mM KH_2PO_4, 10 mM $MgCl_2$, pH 7.4). Cell extracts were used 1:2 with enzyme-specific reaction medium, which changes depending on the enzyme being evaluated. All media contain 50 mM Tris-HCl (pH 7.4) with 5 mM $MgCl_2$, plus 1 mM glucose 6-phosphate and 0.2 mM NADH to evaluate G6PDH activity; 0.2 mM $NADP^+$ with 1 mM malate to determine malic enzyme activity; 0.2 or 1 mM sodium pyruvate to determine LDH isoform M activity; 0.2 mM NAD^+ and 1 mM sodium lactate to determine LDM isoform activity; 0.1 mM NADH with 100 mM ATP, 1 mM fructose 6-phosphate, and 0.1 mM of a mixture of enzymes (aldolase, triose-phosphate isomerase, and glycerophosphate dehydrogenase) to determine PFK activity; 0.15 mM NADH with 100 mM ATP, 20 mM citrate, 10 mM 2-mercaptoethanol, 2 units/ml of malate dehydrogenase, and 0.3 mM of coenzyme-A to determine citrate lyase activity. We measured the presence of reduced NADP (G6PDH and malic), reduction of NAD^+ (LDH), or oxidation of NADH (PFK, citrate lyase) by determining absorbance at 340 nm. To quantify intracellular ATP, cell lysates were subjected to an ATP determination kit (Invitrogen) according to the manufacturer's protocol.

Activities were normalized by cell number or protein mass, following the standard in the literature. Protein quantification of cell lysates was performed by the colorimetric method with a Pierce® BCA protein assay (Thermo Fisher Scientific, Waltham, MA) following the manufacturer's instructions. Samples were read at 562 nm, and results were analyzed by the SoftMax® data acquisition and analysis software (Molecular Devices, Sunnyvale, CA).

Host Gene Expression and M. leprae Viability Analysis by Real-time RT-PCR—Host and Mycobacterial RNA extraction ST88-14 cells were harvested and lysed using TRIzol® reagent, followed by DNase treatment following the manufacturer's instructions (Life Technologies). DNA was extracted as described (41). Nucleic acid samples were quantified using a Nanodrop ND-1000 spectrophotometer, and RNA integrity was analyzed by 1.2% agarose gel electrophoresis.

One microgram of RNA obtained from all cell cultures was reverse transcribed using VILO following the manufacturer's instructions (Life Technologies) in a final volume of 20 μl. Real-time PCR was performed using the SYBR Green PCR Master

Mix (Applied Biosystems, Forster City, CA) following the manufacturer's instructions. All primers used in real-time RT-PCR in the present work were designed by our group from sequences of each reference gene using the Primer3 software version 0.4.0. Sequences were validated by the Primer-Blast tool using the human gene bank of the NCBI. The housekeeping hypoxanthine phosphoribosyltransferase 1 (HPRT1) primer pair was the only exception, bought from Real Time Primers (Elkins Park, PA). To normalize the relative expression of the genes of interest, hypoxanthine phosphoribosyltransferase 1, RPL13 (human ribosomal protein L13), and GAPDH were used as reference genes. Expression values were corrected and quantified by converting the cycle threshold (C_t) value into a numerical value using the following formula: expression value $= 2^{(-\Delta Ct)}$.

M. leprae viability was determined as described elsewhere (41) by the 16S rRNA/16S rDNA ratio determined by real-time PCR performed and read in an ABI StepOne Plus Sequence Detection System (Applied Biosystems).

Evaluation of the Production of Radical Species Using DHE—Schwann cells were maintained in culture under the conditions mentioned above in the absence or presence of 10 μM hydrogen peroxide, 5 μM 6-ANAM, 400 μM BSO, and 50 μM DHE. After being cultured and expanded, 40,000 ST88-14 cells were distributed per well in 24-well plates. After 24 h, cells were exposed to 6-ANAM (inhibitor of G6PDH) or BSO (γ-glutamylcysteine synthetase inhibitor). After 48 h, cells were infected with *M. leprae* or *M. bovis* Moreau with a m.o.i. of 50:1. Seventy hours after seeding, cells were challenged with hydrogen peroxide. Two hours later, cultures were labeled with DHE for 30 min at 37 °C. After 3 washes with cold PBS, cells were harvested with 1% trypsin and transported to a BD FACSAria II (BD Biosciences) in ice-cold PBS plus 10% FBS. Cell suspensions were filtered through a 40-μm net before acquisition. Five thousand events per condition were acquired, and DHE detection was analyzed in PE-A channel after exclusion of events in lumps and dead cells.

Cell Viability—To determine cellular viability, we used two different methods, propidium iodide (PI) microscopy detection and lactate dehydrogenase (LDH) supernatant release. To analyze AMA-treated cells with microcopy, after 36 h of *M. leprae* infection using a m.o.i. of 50:1, coverslip-adherent cells were exposed to AMA at different concentrations for 12 h. After that, 500 nM PI was added to the culture, which was the fixed in 4% paraformaldehyde and DAPI stained after 3 PBS washes. We captured 10 random fields per sample using a Zeiss AxioObserver inverted microscope equipped with a Colibri illuminating system and Plan-Neofluar 40X objective with a numerical aperture of 1.4 (Zeiss, Oberkochen, Germany). The PI red signal was acquired by a monochrome camera HMR Axiocan controlled by Axiovision software version 3.2 (Zeiss, Oberkochen, Germany). The illumination system used a 530-nm LED and Zeiss fluorescence filter 50. Metabolism inhibitor toxicity was determined by LDH release in the culture medium supernatant after treatment at the same conditions used in the experiments: 24 h incubation with 400 μM BSO or 5 μM 6-ANAM, using a Quantification Lactate Dehydrogenase Activity Assay Kit (Labtest, MG, Brazil), according to the manufacturer's protocol.

Electron Microscopy of Human Sciatic Nerve Biopsies—Nerve biopsy samples were obtained from leprosy patients and patients suffering from other neuropathies not related with leprosy, at the Souza Araújo Service at the Oswaldo Cruz Foundation, Rio de Janeiro, Brazil, and were kept frozen at −70 °C until use. For transmission electron microscopy studies, nerve segments were fixed in 2.5% glutaraldehyde diluted in 0.1 M cacodylate buffer followed by post-fixation in 1% osmium tetroxide diluted in the same buffer. The segments were then dehydrated in graded increasing acetone concentrations (from 30 to 100%) and embedded in an Epon resin. Ultrathin transverse sections (60 nm thick) of each nerve were obtained using a Reichert ultramicrotome (Heidelberg, Germany), and sections were collected on copper grids and stained for 30 min in uranyl acetate followed by 10 min in lead citrate. For mitochondrial identification and morphometric analysis, electron micrographs were randomly imaged on a transmission electron microscope Zeiss M-10C operating at 60 KV by a blinded investigator. Five different fields from each nerve were acquired at a ×5,000 magnification, and mitochondria profiles were measured in each field using NIH ImageJ software (42). A total of 127 and 157 mitochondrial profiles were analyzed in nerves obtained from leprosy patients and other non-leprosy neuropathy patients, respectively.

G6PDH Silencing—G6PDH knockdown was achieved in ST88-14 cells by transfection with predesigned small interfering RNAs (siRNA s5446 and s5448) (Life Technologies), here identified as G6PDH#1 and #2, respectively. Cells were transfected with Lipofectamine 2000 according to the manufacturer's instructions (Life Technologies). Six hours after transfection, cells were infected with *M. leprae* for 48 h. Both siRNAs were able to reduce G6PDH expression in ~90%. In contrast, Schwann cell viability was decreased by 10% only. Silencing efficiency, ST88-14 and *M. leprae* viability were determined as described previously in this section.

Statistical Analysis—The results were represented as the mean ± S.E. and statistically evaluated by analysis of variance (ANOVA). The values were considered significant when p was equal to or less than 0.05 ($p < 0.05$). For the statistical analysis of this study, we used GraphPad Prism 5 software.

Ethics Statement—All biopsies were acquired for diagnostic purposes before treatment. The acquisition of all samples was approved by the Ethics Committee of the Oswaldo Cruz Foundation (FIOCRUZ, Rio de Janeiro, RJ, Brazil), license number 170/2012. Written informed consent was voluntarily obtained from each participant.

Author Contributions—R. C. A. M. conducted most of the experiments and analyzed the results. L. R. B. S., K. C. V. G., and F. K. L. C. conducted the oxidative stress and *M. leprae* viability experiments shown in Figs. 5 and 6 and analyzed the results. B. S. M., T. G. T. P., and L. R. B. S. contributed to RT-PCR experiments design and data analysis shown in Figs. 1, 3, and 4. L. S. G., L. S. R., M. G., J. J. A., S. L. G. A., S. C. R., and P. S. R. contributed in experiments design, capture, and analysis in FACS, MALDI, and transmission electron microscopy. E. N. S. and J. A. C. N. recruited and diagnosed leprosy patients, collected samples, and contributed to the study design. M. C. V. P., M. S. P., M. F. O., and M. O. M. contributed to the study design. F. A. L. contributed to the study design, coordination, and wrote the paper.

Acknowledgments—We thank Rudolf Barth, Electron Microscopy Platform of the Oswaldo Cruz Institute/Fiocruz, and Prof. Andre Pedrosa for critical reading and revision.

References

1. WHO. (2015) Weekly epidemiological record. *Wkly. Epidemiol. Rec.* **90,** 461–474
2. Lockwood, D. N., and Suneetha, S. (2005) Leprosy: too complex a disease for a simple elimination paradigm. *Bull. World Health Organ.* **83,** 230–235
3. Lobato, L. S., Rosa, P. S., Ferreira Jda, S., Neumann Ada, S., da Silva, M. G., do Nascimento, D. C., Soares, C. T., Pedrini, S. C., Oliveira, D. S., Monteiro, C. P., Pereira, G. M., Ribeiro-Alves, M., Hacker, M. A., Moraes, M. O., Pessolani, M. C., Duarte, R. S., and Lara, F. A. (2014) Statins increase rifampin mycobactericidal effect. *Antimicrob. Agents Chemother.* **58,** 5766–5774
4. Cole, S. T., Eiglmeier, K., Parkhill, J., James, K. D., Thomson, N. R., Wheeler, P. R., Honoré, N., Garnier, T., Churcher, C., Harris, D., Mungall, K., Basham, D., Brown, D., Chillingworth, T., Connor, R., *et al.* (2001) Massive gene decay in the leprosy bacillus. *Nature* **409,** 1007–1011
5. Mattos, K. A., Oliveira, V. G., D'Avila, H., Rodrigues, L. S., Pinheiro, R. O., Sarno, E. N., Pessolani, M. C., and Bozza, P. T. (2011) TLR6-driven lipid droplets in *Mycobacterium leprae*-infected Schwann cells: immunoinflammatory platforms associated with bacterial persistence. *J. Immunol.* **187,** 2548–2558
6. Mattos, K. A., Lara, F. A., Oliveira, V. G., Rodrigues, L. S., D'Avila, H., Melo, R. C., Manso, P. P., Sarno, E. N., Bozza, P. T., and Pessolani, M. C. (2011) Modulation of lipid droplets by *Mycobacterium leprae* in Schwann cells: a putative mechanism for host lipid acquisition and bacterial survival in phagosomes. *Cell Microbiol.* **13,** 259–273
7. de Mattos, K. A., Sarno, E. N., Pessolani, M. C., and Bozza, P. T. (2012) Deciphering the contribution of lipid droplets in leprosy: multifunctional organelles with roles in *Mycobacterium leprae* pathogenesis. *Mem. Inst. Oswaldo Cruz* **107,** 156–166
8. Nagy, C., and Haschemi, A. (2015) Time and demand are two critical dimensions of immunometabolism: the process of macrophage activation and the pentose phosphate pathway. *Front. Immunol.* **6,** 164
9. Beutler, E. (1996) G6PD: population genetics and clinical manifestations. *Blood Rev.* **10,** 45–52
10. Siegl, C., Prusty, B. K., Karunakaran, K., Wischhusen, J., and Rudel, T. (2014) Tumor suppressor p53 alters host cell metabolism to limit *Chlamydia trachomatis* infection. *Cell Rep.* **9,** 918–929
11. Luzzatto, L., Usanga, F. A., and Reddy, S. (1969) Glucose-6-phosphate dehydrogenase deficient red cells: resistance to infection by malarial parasites. *Science* **164,** 839–842
12. Hsieh, Y. T., Lin, M. H., Ho, H. Y., Chen, L. C., Chen, C. C., and Shu, J. C. (2013) Glucose-6-phosphate dehydrogenase (G6PD)-deficient epithelial cells are less tolerant to infection by *Staphylococcus aureus*. *PloS One* **8,** e79566
13. Matthews, G. M., and Butler, R. N. (2005) Cellular mucosal defense during *Helicobacter pylori* infection: a review of the role of glutathione and the oxidative pentose pathway. *Helicobacter* **10,** 298–306
14. Brown, A. M., Evans, R. D., Black, J., and Ransom, B. R. (2012) Schwann cell glycogen selectively supports myelinated axon function. *Ann. Neurol.* **72,** 406–418
15. Beirowski, B., Babetto, E., Golden, J. P., Chen, Y. J., Yang, K., Gross, R. W., Patti, G. J., and Milbrandt, J. (2014) Metabolic regulator LKB1 is crucial for Schwann cell-mediated axon maintenance. *Nat. Neurosci.* **17,** 1351–1361
16. Warburg, O., Wind, F., and Negelein, E. (1927) The metabolism of tumors in the body. *J. Gen. Physiol.* **8,** 519–530
17. Appelberg, R., Moreira, D., Barreira-Silva, P., Borges, M., Silva, L., Dinis-Oliveira, R. J., Resende, M., Correia-Neves, M., Jordan, M. B., Ferreira, N. C., Abrunhosa, A. J., and Silvestre, R. (2015) The Warburg effect in mycobacterial granulomas is dependent on the recruitment and activation of macrophages by interferon-γ. *Immunology* **145,** 498–507
18. Diaz-Vivancos, P., de Simone, A., Kiddle, G., and Foyer, C. H. (2015) Glutathione-linking cell proliferation to oxidative stress. *Free Radic. Biol. Med.* **89,** 1154–1164
19. Palsson-McDermott, E. M., and O'Neill, L. A. (2013) The Warburg effect then and now: from cancer to inflammatory diseases. *BioEssays* **35,** 965–973
20. Guerreiro, L. T., Robottom-Ferreira, A. B., Ribeiro-Alves, M., Toledo-Pinto, T. G., Rosa Brito, T., Rosa, P. S., Sandoval, F. G., Jardim, M. R., Antunes, S. G., Shannon, E. J., Sarno, E. N., Pessolani, M. C., Williams, D. L., and Moraes, M. O. (2013) Gene expression profiling specifies chemokine, mitochondrial and lipid metabolism signatures in leprosy. *PloS One* **8,** e64748
21. Turrens, J. F. (2003) Mitochondrial formation of reactive oxygen species. *J. Physiol.* **552,** 335–344
22. Douki, T., and Cadet, J. (1996) Peroxynitrite mediated oxidation of purine bases of nucleosides and isolated DNA. *Free Radic. Res.* **24,** 369–380
23. Stocks, J., and Dormandy, T. L. (1971) The autoxidation of human red cell lipids induced by hydrogen peroxide. *Br. J. Haematol.* **20,** 95–111
24. Mailloux, R. J., and Harper, M. E. (2011) Uncoupling proteins and the control of mitochondrial reactive oxygen species production. *Free Radic. Biol. Med.* **51,** 1106–1115
25. Pooya, S., Liu, X., Kumar, V. B., Anderson, J., Imai, F., Zhang, W., Ciraolo, G., Ratner, N., Setchell, K. D., Yoshida, Y., Yutaka, Y., Jankowski, M. P., and Dasgupta, B. (2014) The tumour suppressor LKB1 regulates myelination through mitochondrial metabolism. *Nat. Commun.* **5,** 4993
26. Solenski, N. J., diPierro, C. G., Trimmer, P. A., Kwan, A. L., and Helms, G. A. (2002) Ultrastructural changes of neuronal mitochondria after transient and permanent cerebral ischemia. *Stroke* **33,** 816–824
27. Halestrap, A. P. (1989) The regulation of the matrix volume of mammalian mitochondria *in vivo* and *in vitro* and its role in the control of mitochondrial metabolism. *Biochim. Biophys. Acta* **973,** 355–382
28. Zoratti, M., Szabò, I., and De Marchi, U. (2005) Mitochondrial permeability transitions: how many doors to the house? *Biochim. Biophys. Acta* **1706,** 40–52
29. Rodrigues, L. S., da Silva Maeda, E., Moreira, M. E., Tempone, A. J., Lobato, L. S., Ribeiro-Resende, V. T., Alves, L., Rossle, S., Lopes, U. G., and Pessolani, M. C. (2010) *Mycobacterium leprae* induces insulin-like growth factor and promotes survival of Schwann cells upon serum withdrawal. *Cell. Microbiol.* **12,** 42–54
30. Wisniewski, H. M., and Bloom, B. R. (1975) Primary demyelination as a nonspecific consequence of a cell-mediated immune reaction. *J. Exp. Med.* **141,** 346–359
31. Scollard, D. M., Truman, R. W., and Ebenezer, G. J. (2015) Mechanisms of nerve injury in leprosy. *Clin. Dermatol.* **33,** 46–54
32. Lee, Y., Morrison, B. M., Li, Y., Lengacher, S., Farah, M. H., Hoffman, P. N., Liu, Y., Tsingalia, A., Jin, L., Zhang, P. W., Pellerin, L., Magistretti, P. J., and Rothstein, J. D. (2012) Oligodendroglia metabolically support axons and contribute to neurodegeneration. *Nature* **487,** 443–448
33. Pellerin, L. (2003) Lactate as a pivotal element in neuron-glia metabolic cooperation. *Neurochem. Int.* **43,** 331–338
34. Tekkök, S. B., Brown, A. M., Westenbroek, R., Pellerin, L., and Ransom, B. R. (2005) Transfer of glycogen-derived lactate from astrocytes to axons via specific monocarboxylate transporters supports mouse optic nerve activity. *J. Neurosci. Res.* **81,** 644–652
35. Tang, F., Lane, S., Korsak, A., Paton, J. F., Gourine, A. V., Kasparov, S., and Teschemacher, A. G. (2014) Lactate-mediated glia-neuronal signalling in the mammalian brain. *Nat. Commun.* **5,** 3284
36. Masaki, T., Qu, J., Cholewa-Waclaw, J., Burr, K., Raaum, R., and Rambukkana, A. (2013) Reprogramming adult Schwann cells to stem cell-like cells by leprosy bacilli promotes dissemination of infection. *Cell* **152,** 51–67
37. Domènech-Estévez, E., Baloui, H., Repond, C., Rosafio, K., Médard, J. J., Tricaud, N., Pellerin, L., and Chrast, R. (2015) Distribution of monocarboxylate transporters in the peripheral nervous system suggests putative roles in lactate shuttling and myelination. *J. Neurosci.* **35,** 4151–4156
38. Save, M. P., Shetty, V. P., and Shetty, K. T. (2009) Hypophosphorylation of NF-H and NF-M subunits of neurofilaments and the associated decrease in

KSPXK kinase activity in the sciatic nerves of Swiss white mice inoculated in the foot pad with *Mycobacterium leprae*. *Leprosy Rev.* **80,** 388–401
39. Chiu, S. Y. (2011) Matching mitochondria to metabolic needs at nodes of Ranvier. *Neuroscientist* **17,** 343–350
40. Bohl, L. P., Liaudat, A. C., Picotto, G., Marchionatti, A. M., Narvaez, C. J., Welsh, J., Rodriguez, V. A., and Tolosa de Talamoni, N. G. (2012) Buthionine sulfoximine and 1,25-dihydroxyvitamin D induce apoptosis in breast cancer cells via induction of reactive oxygen species. *Cancer Invest.* **30,** 560–570
41. Martínez-Gutierrez, M., Castellanos, J. E., and Gallego-Gómez, J. C. (2011) Statins reduce dengue virus production via decreased virion assembly. *Intervirology* **54,** 202–216
42. Abràmoff, M. D., Magalhães, P. J., and Ram, S. J. (2004) Image Processing with ImageJ. *Biophotonics Int.* **11,** 36–42